This article has been accepted for publication in a future issue of this journal, but has not been fully edited. Content may change prior to final publication. Citation information: DOI 10.1109/LAWP.2019.2930820, IEEE Antennas and Wireless Propagation Letters

Characterization of Mesoscopic Dielectric Cuboid Antenna at Millimeter-wave Band

Yuuto Samura, Kazuki Horio, Vladimir Antipov, Sergey Shipilov, Aleksandr Eremeev, *Student, IEEE*, Oleg V. Minin, Igor V. Minin, and Shintaro Hisatake, *Member, IEEE*

***Abstract*—Mesoscopic dielectric cuboid antenna (DCA), which can be connected to a standard waveguide, is proposed to achieve high directivity with a simple-structure and low-antenna profile compared with that of a horn antenna of same dimensions. We optimized the antenna dimensions based on simulation to maximize the antenna gain of 14.22 dBi, which is 1.9 dB higher than that of the horn antenna with the same dimensions. Simulation was performed both at 300 GHz and 24 GHz. As a proof-of-concept, we designed and fabricated a scaled DCA with dimensions of $1.2\lambda \times 1.2\lambda \times 1.36\lambda$ and experimentally evaluated the radiation pattern at 24 GHz band. The full width at half maximum (FWHM) values were approximately 21 % and 34 % narrower than those of the horn antenna in the E-plane and H-plane, respectively. The frequency characteristic of sensitivity enhancement using the DCA as the reception antenna shows that the DCA is a nonresonant antenna with a wide bandwidth. Narrower FWHMs of the DCA have been discussed with respect to a two-dimensional near-field phase distribution measured using the electro-optic sensing technique.**

***Index Terms*—Mesoscopic dielectric cuboid, Low-profile antenna, Terahertz wireless communication**

I. Introduction

ELECTROMAGNETIC waves in the millimeter-wave and terahertz (THz) wave band are expected to be employed for future wireless communication because of their availability in a broad bandwidth [1-4]. Regardless of the frequency band, antennas are fundamental components in wireless communication applications. In the past years, various types of millimeter-wave and THz wave antennas have been developed such as metallic lens antenna [5], slot array antennas [6], etc. Particularly in the THz frequency band, the horn antenna has been routinely employed because of its wide bandwidth, connectability to a waveguide, and moderate antenna gain for point-to-point short-range link applications [7-9]. For instance, a low temperature co-fired ceramic (LTCC) horn antenna ($5\lambda \times 5\lambda \times 2.5\lambda$) with a maximum gain of 16 dBi has been demonstrated at 300 GHz band [10]. To take advantage of not only the wide bandwidth but also the short wavelength of the millimeter-wave and THz wave carrier, minimizing the antenna dimension while maintaining the directivity would be desirable.

Y. Samura, K. Horio, and S. Hisatake are with Electrical and Energy System Engineering Division, Gifu University, Gifu City, 501-1193, Japan. (e-mail: hisatake@gifu-u.ac.jp).

V. B. Antipov, S. E. Shipilov, A. I. Eremeev, O. V. Minin, and I. V. Minin are with National Research Tomsk State University, Tomsk, 634050, Russia. (e-mail: prof.minin@gmail.com). O. V. Minin, and I. V. Minin are with Tomsk Polytechnical University, Tomsk, 634050, Russia.

One of the methods to reduce the focal spot involves subwavelength confinement of the millimeter-wave and/or THz wave is to use the so-called effect of photonic terajet generated by three-dimensional (3D) dielectric particle of an arbitrary 3D shape [11, 12]. Recently, we investigated the terajet phenomenon in the near-field regime and employed the mesoscopic dielectric cube as a resolution enhancer in the THz imaging applications [13-15]. This unique phenomenon has been investigated in the near-field regime so far; however, the possibility of the mesoscale dielectric particle application as a far-field antenna has not been reported in the literature yet.

In this letter, we propose the mesoscopic dielectric cuboid antenna (DCA), which has a larger antenna gain compared with that of the horn antenna with the same antenna aperture size and throat length. The structure of the DCA is simple enough to be fabricated by 3D printing or machine milling and is easily connectable to the standard open-ended waveguide. The simulation was made both at 24 GHz and 300 GHz. As a scaled proof-of-concept, we experimentally demonstrated the characteristics of the DCA ($1.2\lambda \times 1.2\lambda \times 1.36\lambda$) at 24 GHz, showing 14.22 dBi of the antenna gain and 21 % and 34 % narrower beam width compared with those of the horn antenna in the E-plane and H-plane, respectively.

This letter is organized as follows: in Section II, the antenna characteristics of the DCA, such as gain and radiation pattern, are compared with those of a horn antenna through the simulation; in Section III, the DCA and the horn antenna are fabricated and near-field distributions are visualized by electro-optic (EO) sensing to demonstrate the advantages of the DCA over the horn antenna; and a conclusion is finally drawn in Section IV.

II. Design and simulation

Fig. 1 shows the simulation model and photograph of a DCA and a horn antenna. In this letter, we compare the radiation characteristics of the DCA with those of the horn antenna with the same antenna dimensions (aperture size of a and throat length of b in Fig. 1). We chose the materials of the DCA and the horn antenna as polytetrafluoroethylene (PTFE) and aluminum, respectively. The DCA has two parts: a cuboid antenna part and a protrusion part (length c) that connects to a standard waveguide. The simulations were conducted using the finite integration technique (CST Microwave Studio software), with the simulation model shown in Fig. 1 (a), in which the protrusion part is connected to the waveguide. In order to match the simulation condition with the experiments, we simulated with the waveguide flange as shown in Fig. 1.

This article has been accepted for publication in a future issue of this journal, but has not been fully edited. Content may change prior to final publication. Citation information: DOI 10.1109/LAWP.2019.2930820, IEEE Antennas and Wireless Propagation Letters

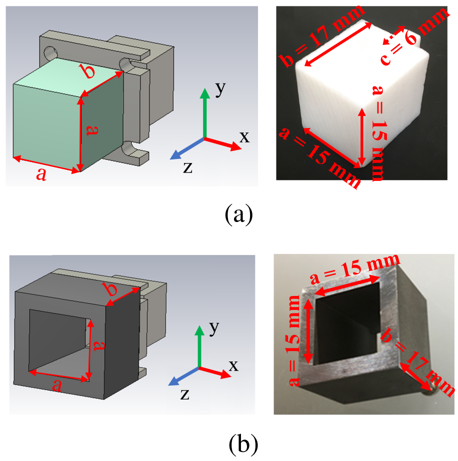

Fig. 1. Fabricated antennas of (a) DCA, and (b) horn antenna. Antennas used in the experiment are sat to a = 15 mm, b = 17 mm, c = 6 mm.

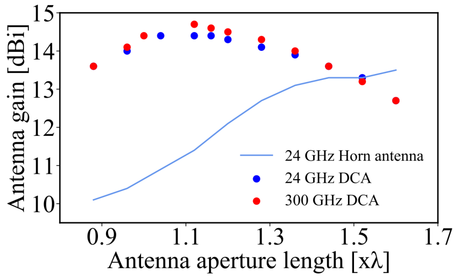

Fig. 2. Simulated antenna gains as a function of the antenna aperture dimension of a.

Fig. 2 shows the simulated antenna gain as a function of the length of the antenna aperture side. The antenna dimension is normalized to the wavelength. The antenna throat length (b in Fig. 1) was set to 1.36λ for both antennas. The simulation was conducted at 24 GHz and 300 GHz for the DCA. We set the relative permittivity and loss tangent of PTFE as 2.1 and 2×10^{-4} at 24 GHz, and 2.0 and 11×10^{-4} at 300 GHz [16], respectively. The loss of aluminum was set as 3.56×10^{7} S/m, which is the electrical conductivity at 24 GHz. Antenna gains of more than 14 dBi can be achieved at around $\lambda < a < 1.3\lambda$ for both frequencies. The maximum antenna gains for the DCA are 14.7 dBi and 14.4 dBi for 300 GHz and 24 GHz, respectively. On the other hand, the antenna gain for the horn antenna was saturated to approximately 13.3 dBi, which is 1.1 dB smaller than the maximum antenna gain of the DCA. The antenna gain of the DCA can reach approximately 20 dBi when the throat length extends approximately 7λ with the aperture size of a = 1.2λ. On the other hand, the maximum gain of 12.6 dBi can be achieved at the throat length of approximately 7λ with the antenna aperture size of a = 1.2λ (see Fig. 1). A decrease in directivity below an aperture size of one wavelength is associated with weak localization of the field at the shadow surface of the dielectric, and that with an aperture size of more than 1.3λ is associated with the field localization inside the dielectric [12-14].

Fig. 3 shows the frequency characteristics of the antenna gain. The simulation was conducted for three situations: (a) open-ended waveguide with flange, (b) DCA, and (c) horn

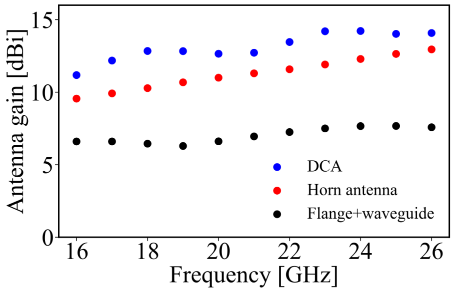

Fig. 3. The frequency characteristics of the antenna gain.

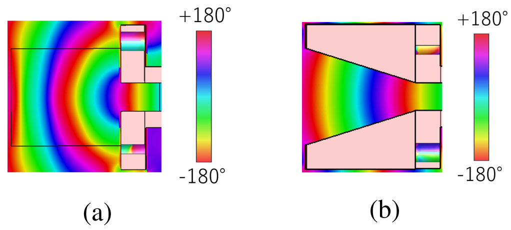

Fig. 4. The phase distribution in each antennas. (a) DCA, (b) horn antenna.

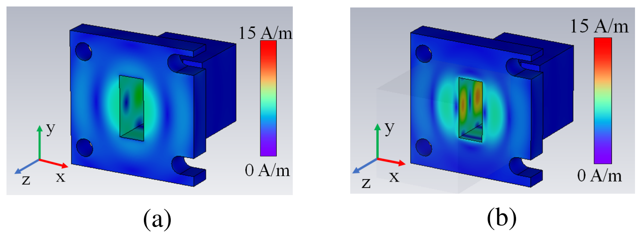

Fig. 5. The current distribution on the flange at 19 GHz. (a) is flange and waveguide only, (b) has the DCA.

antenna. The dimensions of the simulated DCA and horn antenna were a = 15 mm, b = 17 mm, and c = 6 mm, which correspond to a = 1.2λ and b = 1.36λ at 24 GHz. In the entire frequency band, the highest gain was achieved for DCA. The radiation beam width is determined from the effective antenna area and phase distribution.

As discussed later with experimental results, the DCA exhibits a flat phase distribution at the shadow surface of the cube [13, 14]. Fig. 4 shows the phase development inside the antennas. As shown in Fig. 4 (b), the curvature of the wavefront at the end plane of the horn antenna is determined by the geometrical shape of the antenna (length, angle, etc.). In the case of DCA, the wavefront inside the cube near its shadow surface is also determined by the shape of the particle and its refractive index. The phase velocity at the center of the cube is less than that near the dielectric-air boundary [12]. Because of this reason, as shown in Fig. 4 (a), the wavefront at the end of the cube becomes flatter than that for classical horn antenna with the same geometrical dimensions. The collimating effect by a lens is based on the spatial distribution of the optical length. The DCA is made of a dielectric; therefore our technique is a kind of dielectric loading. However the principle of the phase conversion effect is different from that of the conventional lens horn antenna. Moreover, the DCA has an advantage in that it is easy to fabricate.

We also simulated the current distribution on the flange for the three situations (Fig. 5). The simulation was conducted at 19 GHz, where the lowest antenna gain was observed for the

This article has been accepted for publication in a future issue of this journal, but has not been fully edited. Content may change prior to final publication. Citation information: DOI 10.1109/LAWP.2019.2930820, IEEE Antennas and Wireless Propagation Letters

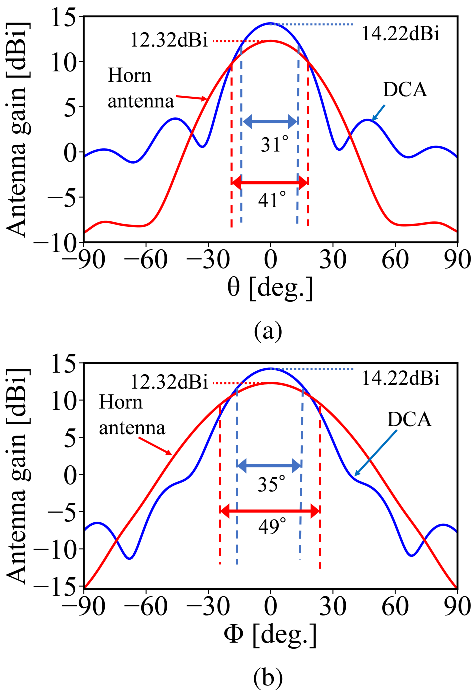

Fig. 6. Simulated far-filed pattern ((a): E-plane and (b): H-plane) of the DCA and horn antenna.

open-ended waveguide with flange. As shown in Fig. 5 (a), the current concentrates near the waveguide and does not spread on the flange surface in the case of the open-ended waveguide with flange. Fig. 5 (b) shows the current distribution when the dielectric cubic particle is placed on the flange surface. In this situation, the current distribution is more uniform than that in the case of the waveguide and flange only. The current transferred to the dielectric also leads to a higher gain and a narrower FWHM in the far field [17]. However, this effect is limited to only a 6 % decrease in the FWHM compared with that in the DCA without the flange.

Fig. 6 shows the simulated far-field pattern of the DCA and the horn antenna. The simulations were conducted at 24 GHz. The dimensions of the simulated DCA and horn antenna were a = 15 mm, b = 17 mm, and c = 6 mm, which correspond to a = 1.2λ and b = 1.36λ at 24 GHz. The 3 dB beam widths (FWHM) of the DCA for the E-plane and H-plane are 31 ° and 35 °, respectively. The FWHM for the horn antenna are 41 ° and 49 ° for the E-plane and H-plane, respectively. The simulation predicted that the FWHMs of the DCA for the E-plane and H-plane are 24 % and 29 % narrower than those of the horn antenna, respectively. However, one drawback for the DCA is a relatively large side-lobe power, as shown in the E-plane in Fig. 6.

III. Experiments

We fabricated the scaled DCA by machine milling. The material used was PTFE. The dimensions of the fabricated DCA were a = 15 mm, b = 17 mm, and c = 6 mm; these correspond to a = 1.2λ and b = 1.36λ at 24 GHz. The DCA was connected to WR-42 open-ended waveguide in the proof-of-concept experiments. We also fabricated the horn antenna with the same antenna aperture size and throat length for the comparison. The horn antenna was made of aluminum and was could also be connected the WR-42 waveguide.

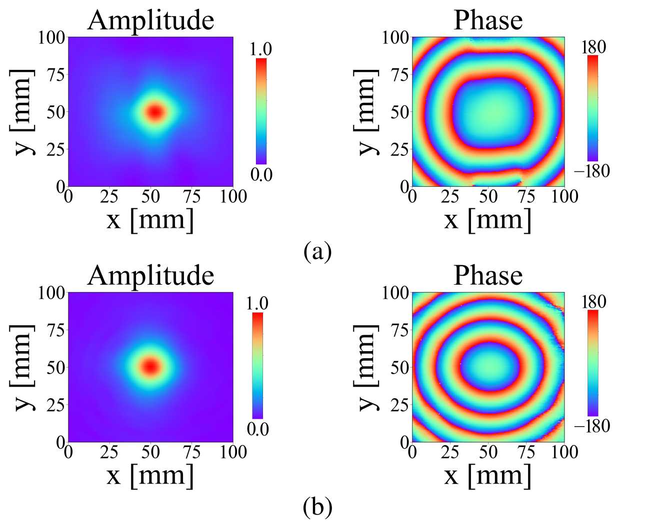

Fig. 7. Measured near-field pattern of (a) DCA and (b) horn antenna.

In the experiment, a 24 GHz signal was generated by a synthesizer (ROHDE&SCHWARZ SMF 100A). The output power was amplified to 20 dBm using a power amplifier and divided by a 5:5 power splitter to monitor the signal power supplied to the antennas. The DCA and the horn antenna were connected to a coaxial-to-waveguide (WR-42) adapter.

Figs. 7 (a) and (b) show the measured antenna near-field pattern (amplitude and phase distributions) for the DCA and the horn antenna, respectively. The frequency was 24 GHz. The measurements were conducted based on the non-polarimetric self-heterodyne EO sensing technique [18,19]. We visualized the two-dimensional amplitude and phase distribution at z = 15 mm, which is the near-field regime for this measurement frequency. The visualized area was 100 mm $\times$ 100 mm. Note that the EO sensor was composed of an organic EO crystal (1 mm $\times$ 1 mm $\times$ 1 mm) with the relative permittivity of 5.76 at 24 GHz. The EO sensor was attached to the optical fiber to form an EO probe. We confirmed by special calibration experiment that the disturbance by the EO probe itself can be neglected. As shown in Fig. 7, the amplitude distributions were similar to each other. However, the phase distributions were quite different, which should lead to different far-field distribution (radiation pattern). To evaluate the phase distribution quantitatively, we show in Fig. 8 the measured one-dimensional phase distribution in the E-plane. As shown in Fig. 8, the curvature radius of the phase distribution for the DCA is larger than that of the horn antenna. The average slopes of the derivatives for the DCA and the horn antenna are -0.50 deg./mm and -0.84 deg./mm, respectively. The slopes calculated from the simulated phase distribution are -0.53 deg./mm and -0.83 deg./mm respectively. The smaller slope of the DCA corresponds to a more plane-wave-like phase front, and it makes narrower beam width.

Figs. 9 (a) and (b) show the far-field pattern (radiation pattern) of the DCA and the horn antenna, respectively, calculated from the measured near-field amplitude and phase distributions. As shown here, the actual radiation pattern of the DCA has very good symmetry. The measured FWHMs for the

This article has been accepted for publication in a future issue of this journal, but has not been fully edited. Content may change prior to final publication. Citation information: DOI 10.1109/LAWP.2019.2930820, IEEE Antennas and Wireless Propagation Letters

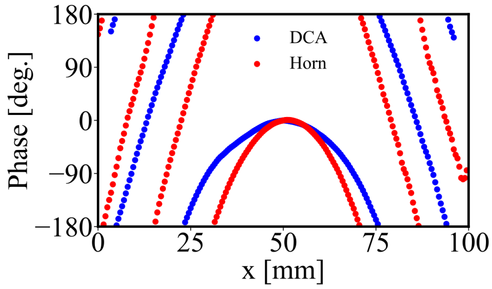

Fig. 8. Measured one-dimensional phase distribution pattern at the near-field regime.

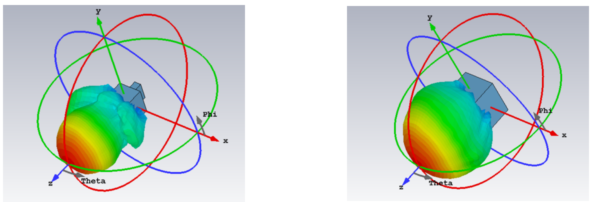

(a) (b)

Fig. 9. Far-field pattern of (a) DCA and (b) horn antenna, calculated from the measured near-field amplitude and phase distributions.

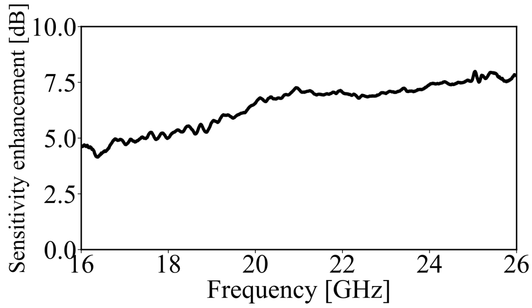

Fig. 10. The sensitivity enhancement when DCA was used as a receiver antenna.

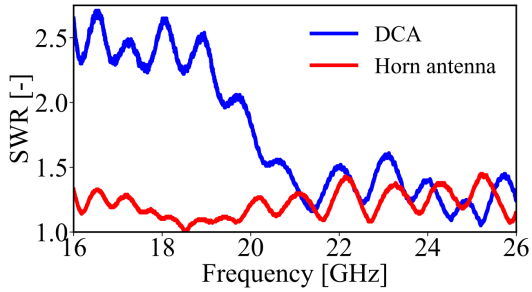

Fig. 11. The SWR of DCA and horn antenna.

DCA are 29.13 ± 0.15 ° and 31.00 ± 0.44 °, for the E-plane and H-plane, respectively, whereas those for the horn antenna are 37.03 ± 0.67 ° for the E-plane and 46.73 ± 0.55 ° for the H-plane. The experimentally obtained FWHMs of the DCA are approximately 21 % and 34 % narrower than those of the horn antenna in the E-plane and H-plane, respectively.

Fig. 10 shows the frequency characteristic of sensitivity enhancement using the DCA as the reception antenna. The characteristic is normalized to the frequency characteristics of the open-ended waveguide with a flange. On the transmitter side, a lens and a conical horn antenna attached to the waveguide were used. The experiment was conducted using a vector network analyzer. Higher enhancement was achieved at the higher frequency region and approximately 7.4 dB enhancement was achieved at 24 GHz. The enhancement by the DCA has no resonant characteristics, indicating a broad-band operation such as that in the horn antennas. This broad-band characteristic is very important for millimeter-wave and THz wireless communication applications. Within the whole frequency band of WR-42, the characteristics of the directivity and the FWHM for the DCA are prominent as compared to that of the horn antenna. The main limitation to extend the operation frequency of the DCA is the loss of the dielectric materials. Although the loss of PTFE slightly increases, the advantages of the DCA such as wide bandwidth, high directivity, and small FWHM with small physical footprint can be exploited in the 300 GHz band.

It should be noted that the observed effect significantly exceeds the possible improvement in the horn transfer coefficient owing to better coordination. For example, the open end of a flanged waveguide has, as a rule, a SWR (Standing Wave Ratio) of 1.5, which corresponds to a return loss of 15 dB (or about 3 %). Thus, the losses to be eliminated owing to mismatch may be in the order of 97 %, or 0.13 dB. Any horn, as a rule, has a smaller SWR than the specified value of 1.5. Fig. 11 shows the measured frequency dependences of the SWR of a DCA and a horn. The SWR of the horn is 1.4 units on average. The SWR of the DCA in the frequency band of 21-26 GHz is approximately 1.2-1.6 units, deteriorating to 2.25-2.7 units in the frequency range of 16-19 GHz. It can be seen that despite the associated increase in mismatch losses of up to 1.03 dB, the sensitivity of the DCA exceeds the sensitivity of the horn by 4.5-5 dB, as shown in Fig. 10. The achievement of DCA gain relative to the horn antenna is confirmed by the results of the near field calculations (Fig. 7), which show that the phase distortions in the front plane of the cuboid are less than those of the horn. Thus, the proposed cubic structure on a scale of wavelength units successfully performs the function of a focusing lens. Another undoubted advantage of the proposed cuboid is that it is easy to manufacture.

IV. Conclusion

We proposed and demonstrated a mesoscopic DCA made of PTFE and directly connected to an open-ended waveguide. Several advantages, including wide bandwidth, connectability to a standard waveguide, higher directivity, and narrower beam width compared with the conventional horn antenna having the same physical volume and size, were demonstrated at 300 GHz and 24 GHz by simulation. We also confirmed in the scale experiment that the FWHMs of the DCA were about 21 % and 34 % narrower than those of the horn antenna in the E-plane and H-plane, respectively; further, a 1.9 dB higher antenna gain compared with the horn antenna at 24 GHz was observed. Note that one practical advantage the DCA has over the horn antenna is that it can protect the open end of the waveguide from the environment and provide feasible (owing to the absence of metal) electromagnetic compatibility. However, these benefits are the subject of further research.

V. Acknowledgment

The work by I.V.M. was carried out within the framework of Tomsk Polytechnic University Competitiveness Enhancement Program.
V.B.A., S.E.S., A.I.E. were supported by the Russian Ministry of Education and Science as a part of the state order No 3.2068.2017/4.6.

VI. Contributions

I.M. and O.M., conceived the idea and supervised the project; V.A., S.Sh., A.E., measured SWR, Y.S., K.H., S.H., performed numerical simulations and experiments; S. H. coordinated and led the project, drafted the manuscript; All authors analyzed the results and contributed to the manuscript.

References

[1] T. Kürner, "Turning THz Communications into Reality: Status on Technology, Standardization and Regulation, " *43rd International Conference on Infrared, Millimeter, and Terahertz Waves*, pp. 1-3, September, 2018.

[2] K. Takano, S. Amakawa, K. Katayama, S. Hara, R. Dong, A. Kasamatsu, I. Hosako, K. Mizuno, K. Takahashi, T. Yoshida, and M. Fujishima, "A 105Gb/s 300GHz CMOS transmitter, " *2017 IEEE International Solid-State Circuits Conference*, pp. 308-309, February, 2017.

[3] H. Hamada, T. Fujimura, I. Abdo, K. Okada, H. Song, H. Sugiyama, H. Matsuzaki, and H. Nosaka, "300-GHz. 100-Gb/s InP-HEMT Wireless Transceiver Using a 300-GHz Fundamental Mixer, " *2018 IEEE/MTT-S International Microwave Symposium-IMS*, pp. 1480-1483, June, 2018.

[4] V. K. Chinni, P. Latzel, M. Zégaoui, C. Coinon, X. Wallart, E. Peytavit, J. F. Lampin, K. Engenhardt, P. Szriftgiser, M. Zaknoune, and G. Ducournau, "Single-channel 100 Gbit/s transmission using III-V UTC-PDs for future IEEE 802.15.3d wireless links in the 300 GHz band, " *Electronics Letters*, vol. 54, No. 10, pp. 638-640, May 17, 2018.

[5] Z. Hao, J. Wang, Q. Yuan, and W. Hong, "Development of a Low-Cost THz Metallic Lens Antenna, " *IEEE Antennas And Wireless Propagation Letters*, vol. 16, pp. 1751-1754, February 20, 2017.

[6] K. Tekkouk, J. Hirokawa, K. Oogimoto, T. Nagatsuma, H. Seto, Y. Inoue, and M. Saito., "Corporate-Feed Slotted Waveguide Array Antenna in the 350-GHz Band by Silicon Process, " *IEEE Transactions on Antennas and Propagation*, vol. 65, No. 1, pp. 217-225, Janualy, 2017.

[7] I. Kallfass, I. Dan, S. Rey, P. Harati, J. Antes, A. Tessmann, S. Wagner, M. Kuri, R. Weber, H. Massler, A. Leuther, T. Merkle, and T. Kürner, "Towards MMIC-Based 300 GHz Indoor Wireless Communication Systems, " *IEICE Transactions on Electronics*, vol. E98.C, No. 12, pp. 1081-1090, December 1, 2015.

[8] T. Nagatsuma, S. Horiguchi, Y. Minamikata, Y. Yoshimizu, S. Hisatake, S. Kuwano, N. Yoshimoto, J. Terada, and H. Takahashi, "Terahertz wireless communications based on photonics technologies, " *Optics Express*, vol. 21, No. 20, pp. 23736-23747, 2013.

[9] T. Tajima, H. Song, and M. Yaita, "300-GHz Microstrip-to-Waveguide Transition on a Polyimide Substrate Integrated with an LTCC Substrate Integrated Waveguide, " *IEICE Transactions on Electronics*, vol. E98.C, No. 12, pp. 1120-1127, 2015.

[10] T. Takuro, H. Song, M Yaita, K. Ajito, and N. Kukutsu, "300-GHz LTCC horn antennas based on antenna-in-package technology, " *European Microwave Conference*, pp. 231-234, 2013.

[11] I. V. Minin, and O. V. Minin, "Photonics of isolated dielectric particles of arbitrary three-dimensional shape-a new direction of optical information technology, " *Vestnik NGU Series: Information Technologies*, vol. 12, No. 4, pp. 59-70, 2014 (in Russian).

[12] I. V. Minin, and O. V. Minin, "Resolution Below the Diffraction Limit, " *Diffractive Optics and Nanophotonics*, Springer, Berlin, 2016.

[13] H. H. Nguyen Pham, S. Hisatake, I. V. Minin, O. V. Minin, and T. Nagatsuma, "Three-dimensional direct observation of Gouy phase shift in a terajet produced by a dielectric cuboid, " *Applied Physics Letters*, vol. 108, No. 19, pp. 191102, May, 2016

[14] H. H. Nguyen Pham, S. Hisatake, O. V. Minin, T. Nagatsuma, and I. V. Minin , "Asymmetric phase anomaly of terajet generated from dielectric cube under oblique illumination, " *Applied Physics Letters*, vol. 110, pp. 201105, 2017.

[15] H. H. Nguyen Pham, S. Hisatake, O. V. Minin, T. Nagatsuma, and I. V. Minin, "Enhancement of spatial resolution of terahertz imaging systems based on terajet generation by dielectric cube, " *APL Photonics*, vol. 2, No. 5, pp. 056106, May 11, 2017.

[16] B. Stöckel, "Quasi-optical measurement of complex dielectric constant at 300 GHz, " *International Journal of Infrared and Millimeter Waves*, vol. 14, No. 10, pp. 2131-2148, October, 1993.

[17] A. Munir, Y. P. Saputra, and Y. Y. Maulana, "Experimental approach of X-band slotted microstrip patch antenna array with non-uniform current distribution, " *International Conference on Electromagnetics in Advanced Applications (ICEAA)*, pp. 764-767, September, 2016.

[18] S. Hisatake, H. H. Nguyen Pham, and T. Nagatsuma, "Visualization of the spatial-temporal evolution of continuous electromagnetic waves in the terahertz range based on photonics technology, " *Optica*, vol. 1, No. 6, pp. 365-371, 2014.

[19] S. Hisatake, H. Nakajima, H. H. Nguyen Pham, H. Uchida, M. Tojyo, Y. Oikawa, K. Miyaji, and T. Nagatsuma, "Mapping of electromagnetic waves generated by free-running self-oscillating devices, " *Scientific Reports*, vol. 7, No. 1, pp. 9203, June 28, 2017.